

Macroscopic model for analyzing the electro-optics of uniform lying helix cholesteric liquid crystals

Guanjun Tan,¹ Yun-Han Lee,¹ Fangwang Gou,¹ Minggang Hu,² Yi-Fen Lan,³ Cheng-Yeh Tsai,³ and Shin-Tson Wu^{1,a)}

¹College of Optics and Photonics, University of Central Florida, Orlando, Florida 32816, USA

²Xi'an Modern Chemistry Research Institute, Xi'an 710065, China

³AU Optronics Corporation, Hsinchu 30078, Taiwan

(Received 5 March 2017; accepted 18 April 2017; published online 1 May 2017)

A macroscopic model is developed for analyzing the electro-optics of short-pitch uniform lying helix (ULH) cholesteric liquid crystals (CLCs). Both flexoelectric effect and dielectric effect make important contributions to the maximum transmittance and operation voltage of the ULH devices. Based on the proposed macroscopic approximation, we derive an analytical expression to quantitatively evaluate the relative strength of these two effects. Very good agreement between theory and experiment is achieved. We also investigate the viewing angle of ULH CLC displays and find that their viewing angle characteristics are similar to those of conventional in-plane switching liquid crystal displays. *Published by AIP Publishing.* [<http://dx.doi.org/10.1063/1.4982761>]

I. INTRODUCTION

Thin-film-transistor liquid crystal displays (TFT LCDs)¹ have been widely used in TVs, computers, and smartphones, due to their low cost, long lifetime, and wide color gamut when quantum-dot (QD) backlight is employed.^{2,3} However, lately LCD is facing strong competition from organic light emitting diode (OLED) displays. In particular, LCD suffers about 100× slower response time than OLED; thus, its image blur for the fast-moving objects is more noticeable. Recent studies indicate that if an LC response time is shorter than 2 ms, then its motion picture response time would be comparable to that of OLED.^{4,5} To achieve fast response time, several approaches have been investigated, such as polymer-stabilized blue phase liquid crystals (BPLC),^{6,7} chiral nanostructured devices,⁸ and short-pitch cholesteric liquid crystals (CLCs) based on flexoelectric effect.^{9–11}

Flexoelectric effect was first discovered by Meyer in 1969.⁹ It describes the coupling between electric polarization and splay-bend elastic distortions in nematic LCs. Generally, the flexoelectric polarization can be expressed as

$$\mathbf{P}_f = e_s \hat{\mathbf{n}} (\nabla \cdot \hat{\mathbf{n}}) - e_b \hat{\mathbf{n}} \times (\nabla \times \hat{\mathbf{n}}), \quad (1)$$

where e_s and e_b stand for the splay and bend flexoelectric coefficient, respectively, and $\hat{\mathbf{n}}$ is the unit vector of LC director. This effect directly relates the electric field with the LC director's curvature. Thus, a splay-bend pattern can be induced by the applied electric field through flexoelectric effect. Later, a periodic splay-bend pattern in the CLC can also be produced if the electric field is perpendicular to the helical axis.¹⁰ Such an electric field-induced splay-bend distortion exerts a torque to rotate the helix axis, known as helical flexoelectric effect. Correspondingly, the optical axis shows unique uniform in-plane switching (IPS).¹⁰ In experiment, the induced rotation angle of the helical axis is

approximately linear to the electric field.^{10,12} Later, a more detailed theoretical model was developed.^{13–15} The rotation angle is correlated with the applied field as¹⁵

$$\tan \Psi = \frac{p}{2\pi} \frac{e_s - e_b}{2K_{22}} E - \frac{K_{11} - 2K_{22} + K_{33}}{2K_{22}} \sin \Psi, \quad (2)$$

where Ψ is the rotation angle of the helix axis, p is the pitch length of the CLC, E is the applied electric field, and K_{11} , K_{22} , and K_{33} are the splay, twist, and bend elastic constants. When E is weak, Ψ is small so that $\sin \Psi \approx \tan \Psi \approx \Psi$, and then the equation can be reduced to a linear form, which is consistent to the experimental observation.

The dynamic response of flexoelectro-optic effect was also studied, and the response time has the following form:¹⁶

$$\tau = \frac{\gamma}{K} \frac{p^2}{4\pi^2}, \quad (3)$$

where γ is the effective viscosity associated with the distortion of the helix, K is the effective elastic constant which can be simplified to $(K_{11} + K_{33})/2$ under one-elastic-constant assumption.^{13,14} For a short-pitch CLC whose pitch length is usually shorter than 300 nm, the flexoelectro-optic response time is in the sub-millisecond region.^{16,17} Such a fast response time makes flexoelectro-optic effect a strong candidate for field sequential color displays,^{18,19} and fast-switching photonic applications.²⁰

Some bimesogenic^{17,21–23} and bent-core²⁴ LC materials possess a large flexoelastic coefficient, which helps to reduce the operation voltage and enlarge the rotation angle of the helix axis. However, these bimesogenic materials usually have a small but positive dielectric anisotropy,²² which would couple the dielectric effect into the LC device. The dielectric coupling is supposed to influence the electro-optical performance of the material. Some experimental observations have already demonstrated such influence.^{14,23} Therefore, in a rigorous theoretical analysis, the coupling of these two effects has to be taken into consideration.

^{a)}Electronic mail: swu@ucf.edu

In this paper, we investigate the coupling between flexoelectric effect and dielectric effect, both theoretically and experimentally. In Sec. II, we develop a macroscopic model for analyzing the electro-optic properties of a short-pitch cholesteric LC. The underlying physical mechanisms are described. Further, an analytical expression is derived to quantitatively evaluate the relative strength of these two electro-optic effects. In Sec. III, we perform experiment to validate the proposed macroscopic model. For display devices, wide viewing angle is an important requirement. In Sec. IV, we simulate the viewing angle of a flexoelectric device called uniform lying helix (ULH) LC cell. We find that its viewing angle characteristic is similar to that of in-plane switching (IPS) LCD. The viewing cone of ULH LC can be widened by two compensation methods.

II. THEORETICAL ANALYSIS

A. Liquid crystal director

To simulate the electro-optic properties of a LC device, we need to calculate the LC director distribution first. For a CLC with undistorted helical structure, we assume the helix axis is along z axis with a pitch length p . To couple flexoelectric effect into the director reorientation, the electric field should be perpendicular to the helix axis. Without losing the generality, let us assume the \mathbf{E} field is along x axis. Under such a condition, the free energy density is given by

$$\begin{aligned} f = & \frac{1}{2}K_{11}(\nabla \cdot \hat{\mathbf{n}})^2 + \frac{1}{2}K_{22}(\hat{\mathbf{n}} \cdot \nabla \times \hat{\mathbf{n}} + k)^2 \\ & + \frac{1}{2}K_{33}(\hat{\mathbf{n}} \times \nabla \times \hat{\mathbf{n}})^2 - e_s \mathbf{E} \cdot \hat{\mathbf{n}}(\nabla \cdot \hat{\mathbf{n}}) \\ & + e_b \mathbf{E} \cdot \hat{\mathbf{n}} \times \nabla \times \hat{\mathbf{n}} - \frac{1}{2}\epsilon_0 \Delta\epsilon (\mathbf{E} \cdot \hat{\mathbf{n}})^2, \end{aligned} \quad (4)$$

where K_{11} , K_{22} , and K_{33} are the splay, twist, and bend elastic constants, respectively, k is the twist of the chiral structure which is defined as $2\pi/p$, \mathbf{E} is the applied electric field, ϵ_0 is the vacuum permittivity, and $\Delta\epsilon$ is the dielectric anisotropy of the LC material. The first three terms in Eq. (4) represent elastic energy, which is independent of electric field. The fourth and fifth terms are from flexoelectric effect, corresponding to the flexoelectric polarization in Eq. (1). The last term is from the dielectric effect. In our Cartesian coordinate system, $\hat{\mathbf{n}} = (\cos\theta \cos\phi, \cos\theta \sin\phi, \sin\theta)$, where θ is the molecular tilt angle between LC director and x - y plane and ϕ is the twist angle between director's projection in x - y plane and x axis. The θ and ϕ are functions of z coordinate. Strictly speaking, there is small distortion of the helical pitch length under the applied field.^{14,25} While given that the pitch is much shorter than wavelength, the macroscopically optical behaviors should only depend on the relative distribution of the molecules within one pitch, instead of the total pitch length. So, the influence of pitch distortion on macroscopic optical behavior is small and can be neglected in our macroscopic optical simulations. To make it accurate, in the following analysis, the z coordinate is scaled by the pitch length, namely, $\tilde{z} = z/p$.²⁵

In ULH cells, we should mainly focus on the bulk behavior. Therefore, the surface anchoring effect contribution to the free energy is reasonably ignored.²⁵ The simulation for bulk behavior of CLC ULH cell can be further simplified to one pitch with periodic expansion. Then, the LC director distribution can be numerically obtained by minimizing the free energy with Euler-Lagrange equations and fixed boundary conditions.²⁵ By substituting the free energy expression into Euler-Lagrange equations, two differential equations are obtained

$$\begin{aligned} 0 = & \frac{d^2\theta}{d\tilde{z}^2} \cdot (K_{11} \cos^2\theta + K_{33} \sin^2\theta) + \left(\frac{d\theta}{d\tilde{z}}\right)^2 \\ & \cdot \frac{1}{2} \sin(2\theta)(-K_{11} + K_{33}) + \left(\frac{d\phi}{d\tilde{z}}\right)^2 \\ & \cdot \sin(2\theta) \left[K_{22} \cos^2\theta - \frac{1}{2}K_{33} \cos(2\theta) \right] \\ & + \frac{d\phi}{d\tilde{z}} \cdot \left[(e_1 - e_3)E \cos^2\theta \sin\phi - kK_{22} \sin(2\theta) \right] \\ & - \frac{1}{2}\epsilon_0 \Delta\epsilon E^2 \cos^2\phi \sin(2\theta), \end{aligned} \quad (5a)$$

$$\begin{aligned} 0 = & \frac{d^2\phi}{d\tilde{z}^2} \cdot \cos^2\theta (K_{22} \cos^2\theta + K_{33} \sin^2\theta) \\ & + \frac{d\theta}{d\tilde{z}} \frac{d\phi}{d\tilde{z}} \cdot \sin(2\theta) \left[-2K_{22} \cos^2\theta + K_{33} \cos(2\theta) \right] \\ & + \frac{d\theta}{d\tilde{z}} \cdot \left[kK_{22} \sin(2\theta) - (e_1 - e_3)E \cos^2\theta \sin\phi \right] \\ & - \frac{1}{2}\epsilon_0 \Delta\epsilon E^2 \cos^2\theta \sin(2\phi). \end{aligned} \quad (5b)$$

With fixed boundary conditions²⁵ and the appropriate material parameters^{11,17} listed in Table I, we can obtain the LC director distribution along helix axis by numerically solving Eqs. (5a) and (5b). Results on the LC director distribution in one pitch are plotted in Fig. 1. From Fig. 1, we can see clearly how the dielectric anisotropy affects the flexoelectric effect. When $\mathbf{E} = 0$ [Figs. 1(a) and 1(d)], the LC directors are twisted along helix axis, same as conventional CLC structure. With $\mathbf{E} = 15 \text{ V}/\mu\text{m}$ and $\Delta\epsilon = 0$, based on the initial twist arrangement the flexoelectric effect makes the LC directors to tilt uniformly [Figs. 1(b) and 1(e)]. If the LC host has $\Delta\epsilon = 5$, then both flexoelectric effect and dielectric effect co-exist; the latter causes some distortion to the uniform tilt induced by the flexoelectric effect [Fig. 1(c)]. Under such a condition, the LC

TABLE I. Material parameters used for the simulation in this work.

Material parameter	Symbol and value
Splay elastic constant	$K_{11} = 7.0 \text{ pN}$
Twist elastic constant	$K_{22} = 3.5 \text{ pN}$
Bend elastic constant	$K_{33} = 7.0 \text{ pN}$
Splay flexoelectric coefficient	$e_s = 10 \text{ pC/m}$
Bend flexoelectric coefficient	$e_b = -10 \text{ pC/m}$
Dielectric anisotropy	$\Delta\epsilon = 0$
Ordinary refractive index	$n_o = 1.50$
Extraordinary refractive index	$n_e = 1.65$
Pitch length	$p = 300 \text{ nm}$

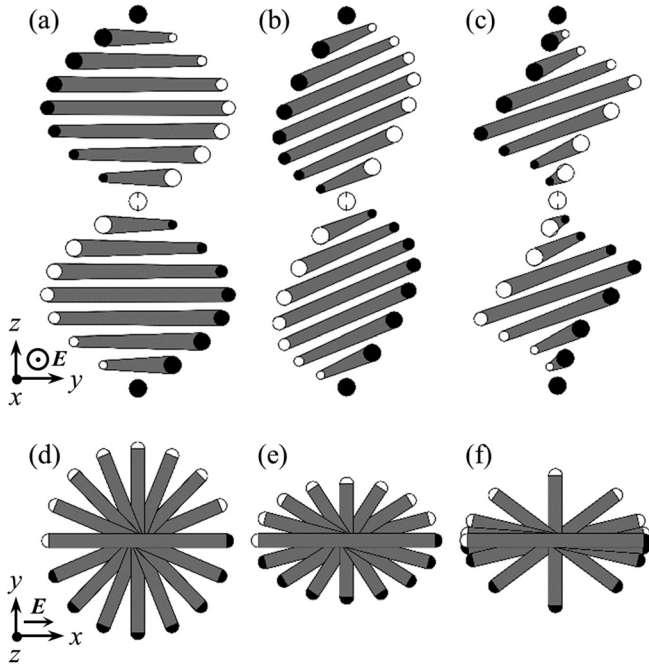


FIG. 1. LC director distribution within one pitch. (a), (b), and (c) are viewed along x axis and (d), (e), and (f) are along z axis. (a) (d): $\mathbf{E}=0$; (b) (e): $\Delta\epsilon=0$ and $\mathbf{E}=15 \text{ V}/\mu\text{m}$ in x direction; (c), (f): $\Delta\epsilon=5$ and $\mathbf{E}=15 \text{ V}/\mu\text{m}$ in x direction.

directors are pulled toward the electric field direction due to the dielectric effect [Fig. 1(f)].

B. Macroscopic model

The LC director distribution essentially determines the macroscopic optical performance. The flexoelectric effect and dielectric effect finally manifest themselves through the macroscopic optical properties. When the pitch length is smaller than the wavelength, the periodic helical-shaped dielectric medium can be treated as a macroscopically homogeneous (HG) medium.^{14,26} The macroscopic model for a static short-pitch CLC has been discussed in previous publications,^{26,27} but the macroscopic approximation for CLCs with large flexoelectric effect and dielectric effect has not been investigated previously. So, in this section, we extend the macroscopic approximation to the dynamic process with an electric field applied.

It is usually very difficult to obtain the analytical expressions for the refractive indices and orientation of the macroscopically effective medium,^{26,27} especially for the CLCs with flexoelectric effect.²⁵ Previous pioneering investigation¹⁴ gave the basic understanding of dielectric coupling. But the previous simplified model was limited by accuracy and uniformity of LC director tilt. Some previous works^{10,13} briefly discussed the basic inter-coupling mechanism between flexoelectric effect and dielectric effect, with simplified theoretical analysis, but the optical behaviors were not presented. Here, we propose a numerical method based on finite element method (FEM) in frequency domain. First, we need to construct a thin LC film whose LC director distribution is calculated from the Euler-Lagrange equations [Eqs. 5(a) and 5(b)]. After a linearly polarized incident electromagnetic wave propagates through

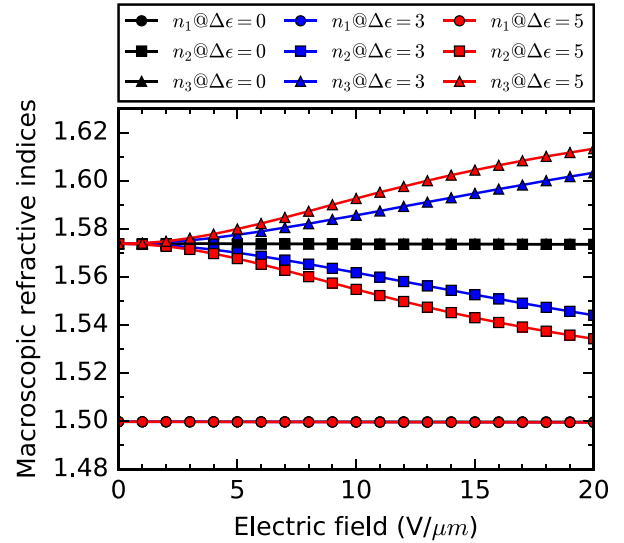


FIG. 2. Effective principal refractive indices obtained from our macroscopic model. The material parameters are listed in Table I. Three cases with different dielectric effect strengths are presented: $\Delta\epsilon=0, 3$ and 5 . Three n_1 curves coincide at ~ 1.50 , and the n_2 and n_3 curves for $\Delta\epsilon=0$ also completely overlap.

such a thin LC film, the phase retardation is recorded. With different phase retardations of a series of incident waves with different polarization directions, we are able to determine the orientation of the effective optic axes and principal refractive indices. With the material parameters listed in Table I, the effective refractive indices and orientation, which is represented by the rotation angle of the effective optic axis, are illustrated in Figs. 2 and 3. To be consistent with our experiments, we use $\lambda=488 \text{ nm}$ in the simulation.

The numerical results from our macroscopic model present a clear physical picture on the working mechanisms of flexoelectric effect and dielectric effect. The role of flexoelectric effect is mainly to rotate the optic axis as shown in Fig. 3. The rotation angle of the material with purely flexoelectric effect, i.e., $\Delta\epsilon=0$, matches well with the analytical results [Eq. (2)]. While the dielectric effect affects the electro-optics of ULH in two ways: (1) it helps elongate the refractive index ellipsoid along the electric field direction, as depicted in Fig. 2. The principal refractive index along the electric field direction, namely, n_3 , increases with \mathbf{E} , but n_2

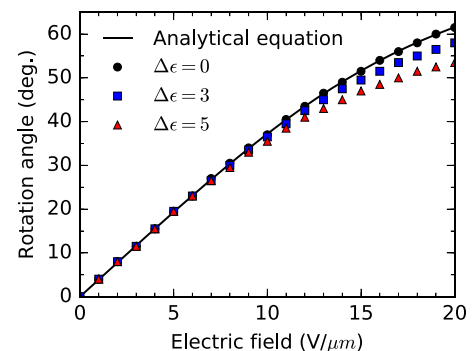


FIG. 3. Simulated electric field-induced rotation angle of the macroscopic optic axis with our macroscopic model. The material parameters are listed in Table I. Three cases with different dielectric anisotropies are presented: $\Delta\epsilon=0, 3$ and 5 . The analytical equation employed is Eq. (2).

(the refractive index perpendicular to \mathbf{E}) decreases. As a result, the effective birefringence $\Delta n = n_2 - n_1$ decreases as \mathbf{E} increases. Actually, this phenomenon is quite similar to the Kerr effect of blue phase liquid crystal,^{28,29} which is also caused by dielectric effect. And now the macroscopic refractive index ellipsoid is biaxial, which is different from conventional uniaxial nematic LC. (2) The dielectric effect makes the LC director reorientation nonuniform, which in turn slightly decreases the rotation angle in the strong electric field region, as Fig. 3 shows. Such a rotation angle decrease induced by dielectric coupling has been investigated previously,³⁰ which would also change the final electro-optic (E-O) performance. As will be discussed later, the impact of this decreased rotation angle is much smaller than that of reduced effective birefringence.

C. Voltage-transmittance curve

To verify our model, we simulate the electro-optic effect of a uniform lying helix (ULH) CLC cell with and without macroscopic approximation. In an ULH cell, the helix axis is uniformly aligned parallel to the substrate, and the applied electric field is perpendicular to the helix axis. The ULH cell is sandwiched between two crossed polarizers, with initial helix axis parallel to the absorption axis of one of the crossed polarizers. In our experiment, the cell gap was controlled at $d = 3.3 \mu\text{m}$ and wavelength at $\lambda = 488 \text{ nm}$.

With macroscopic approximation, the ULH cell is equivalent to an effective homogenous medium. Then the voltage-dependent transmittance (VT) of a ULH cell can be calculated from

$$T = \sin^2\left(\frac{\pi\Delta n d}{\lambda}\right) \cdot \sin^2(2\Psi), \quad (6)$$

where $\Delta n = n_2 - n_1$ is the effective birefringence shown in Fig. 2, and Ψ is the rotation angle of the optic axis plotted in Fig. 3.

We can also carry out the optical simulation directly based on the LC director distribution, without any approximation. From the Euler-Lagrange equations, the LC director distribution in one pitch is obtained. The bulk director distribution is constructed by the periodic expansion. Then, optical simulation is performed based on the constructed LC director in the whole cell. We use FEM method in the optical simulation. The simulated VT curves are displayed in Fig. 4. Good agreement between these two methods is achieved. Thus, our proposed macroscopic approximation is validated. In the VT curve, the applied voltage corresponding to peak transmittance is called on-state voltage. From Fig. 4, a larger $\Delta\epsilon$ tends to reduce the maximum transmittance but the on-state voltage is also lowered. The respective contributions of flexoelectric effect and dielectric effect are clearly distinguished in Fig. 4. The first term in Eq. (6) decreases as V increases because of effective birefringence change induced by the dielectric effect. The second term is mainly induced by the flexoelectric effect, and it is insensitive to the $\Delta\epsilon$ value. So, the decreased peak transmittance and on-state

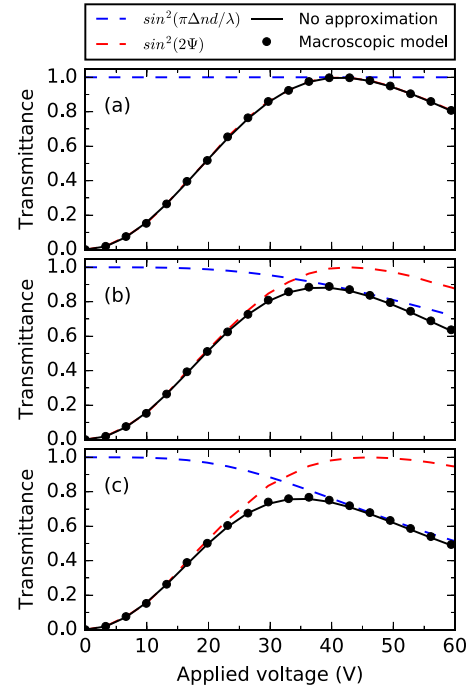


FIG. 4. Simulated VT curves with and without macroscopic approximation. Material parameters are listed in Table I. Three $\Delta\epsilon$ values are simulated: (a) $\Delta\epsilon = 0$, (b) $\Delta\epsilon = 3$, and (c) $\Delta\epsilon = 5$. The blue dashed lines represent the first term of Eq. (6), and the red dashed lines represent the second term.

voltage is mainly attributed to the dielectric effect, more specifically, the decrease of Δn in the first term of Eq. (6).

In order to quantitatively evaluate the dependence of effective birefringence Δn on the electric field, detailed theoretical analysis also needs to be implemented. Let us start from the pure dielectric effect, specifically the quadratic Kerr effect, in CLCs or BPLCs.^{8,28} That is a special case of Eqs. (5a) and (5b) without the flexoelectric effect. With flexoelectric coefficients $e_s = e_b = 0$ and induced tilt angle $\theta = 0$, Eq. (5a) can degenerate to an identity equation, and Eq. (5b) is simplified to

$$\frac{d^2\phi}{d\tilde{z}^2} = \frac{\epsilon_0\Delta\epsilon p^2}{2K_{22}} E^2 \sin(2\phi), \quad (7)$$

where $\tilde{z} = z/p$ is the normalized coordinate and p is the pitch length. The quadratic dependence on electric field is clearly revealed in Eq. (7). The quadratic coefficient is then defined as Kerr constant.²⁹ A solution to the differential equation (7) was already given in a previous work,²⁵ which can be expressed by Jacobi-amplitude function. Here, we skip the complicated derivation processes. One should notice that the LC director distribution $\phi(\tilde{z})$ only depends on the coefficient $\epsilon_0\Delta\epsilon p^2 E^2 / K_{22}$ in Eq. (7). Thus, the macroscopically effective birefringence Δn is only a function of $\epsilon_0\Delta\epsilon p^2 E^2 / K_{22}$. Considering the intrinsic birefringence of an LC, the effective birefringence Δn can be expressed as

$$\Delta n = \Delta n_0 \cdot \mathcal{F}\left(\frac{\epsilon_0\Delta\epsilon p^2}{K_{22}} E^2\right), \quad (8)$$

where Δn_0 is the LC's intrinsic birefringence and $\mathcal{F}(x)$ is a function correlating the electric field with the induced

effective birefringence. The $\mathcal{F}(x)$ can be calculated by the macroscopic model and results are plotted in Fig. 5. This curve is similar to the extended Kerr model in BPLCs.²⁸

If the flexoelectric effect and the dielectric effect co-exist, then the change in the effective birefringence and optic axis rotation would also occur simultaneously. To exclude the effect of optic axis rotation, we need to make the coordinate system transformation. For each effective optic axis rotation angle, noted as Ψ in Eq. (2), we rotate the coordinate system by an angle Ψ correspondingly, to place all coordinate axes just on the optic axes. The old coordinate system space is denoted as $S_1(\theta, \phi)$, and after transformation, the new coordinate space is $S_2(\alpha, \beta)$. With the two-elastic-constant approximation $K_{11} = K_{33} \neq K_{22}$, after the same simplification procedure used in Eq. (7), we obtain the Euler-Lagrange equation in new coordinate space

$$\frac{d^2\alpha}{dz^2} = \frac{\varepsilon_0\Delta\epsilon p^2}{2(K_{11}\sin^2\Psi + K_{22}\cos^2\Psi)} E^2 \sin(2\alpha), \quad (9)$$

where α is the twist angle in new coordinate space just like ϕ in old coordinate system and Ψ is the rotation angle of optic axis as shown in Eq. (2) and Fig. 3. By comparing Eqs. (7) and (9), the only difference is the quadratic coefficient. The flexoelectric effect is introduced into Eq. (9) by the rotation angle Ψ in the coefficient. That gives us a deeper understanding on the working mechanisms of the dielectric effect and the flexoelectric effect. The effective birefringence change is mainly induced by the dielectric effect, through the LC director reorientation under electric field. Meanwhile, the flexoelectric effect tends to rotate the LC directors uniformly and keep the director in a helical configuration.^{10,13} The interaction and competition of these two effects yield to the final molecular distribution. Then, our proposed macroscopic optical model directly relates these two effects with final optical behaviors. As a result, the effective birefringence and the optic axis rotation is jointly determined by the flexoelectric effect and the dielectric effect, which in turn gives new physical understanding in comparison with previous work.^{10,14}

After the abovementioned theoretical analysis, the transmittance of the ULH cell can be further detailed as

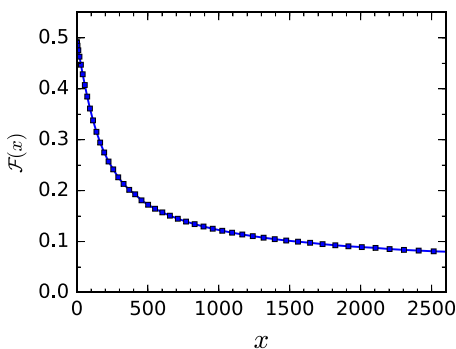


FIG. 5. The $\mathcal{F}(x)$ curve calculated from our macroscopic model. The function is to relate the electric field and induced effective birefringence change. The argument in this function represents a dimensionless quantity $\varepsilon_0\Delta\epsilon p^2 E^2 / K_{22}$.

$$T = \sin^2 \left[\frac{\pi d}{\lambda} \Delta n_0 \mathcal{F} \left(\frac{\varepsilon_0 \Delta \epsilon p^2 E^2}{K_{11} \sin^2 \Psi + K_{22} \cos^2 \Psi} \right) \right] \times \sin^2 [2\Psi(E)], \quad (10)$$

where $\mathcal{F}(x)$ is the function from Eq. (8) and $\Psi(E)$ is the rotation angle of the optic axis. Next, we validate Eq. (10) by further numerical simulation. Figure 6 shows the results from analytical equation [Eq. (10)] and non-approximate numerical simulation. The VT curves obtained from numerical and analytical methods agree well with each other. One may notice that there is a small discrepancy for $\Delta\epsilon = 5$ in Fig. 6. That can be explained by the small decrease of the in-plane rotation angle induced by dielectric coupling, as shown in Fig. 3.

D. Figure of merit (FOM)

The dielectric coupling in ULH cell decreases maximum transmittance and on-state voltage, as clearly shown in Fig. 6. Some prior experiments have been conducted to investigate the dielectric coupling effect.^{14,30} Here, we quantitatively analyze the dielectric coupling with our proposed macroscopic model.

In Eq. (10), the first term is related to birefringence which is proportional to \mathbf{E}^2 , and in the second term the rotation angle is linear to \mathbf{E} . Based on that, we propose a quantity to evaluate the relative strength of the flexoelectric effect and dielectric effect. We define a figure of merit (*FOM*) as

$$FOM = \frac{(e_s - e_b)^2 (K_{11} + 2K_{22} + K_{33})}{\varepsilon_0 \Delta \epsilon (K_{11} + K_{33})^2}. \quad (11)$$

Such a *FOM* is dimensionless; it increases with the flexoelectric effect but decreases with the dielectric effect. After we have defined the *FOM*, it is necessary to verify that the proposed definition is reasonable and can be used to predict the E-O performance. Therefore, we relate *FOM* directly with the corresponding VT curves. We have considered hundreds of LC mixtures with reasonable flexoelectric coefficients, dielectric anisotropies, elastic constants, etc. With the help of macroscopic model, namely, by Eq. (10), the VT simulation can be accomplished accurately and quickly.

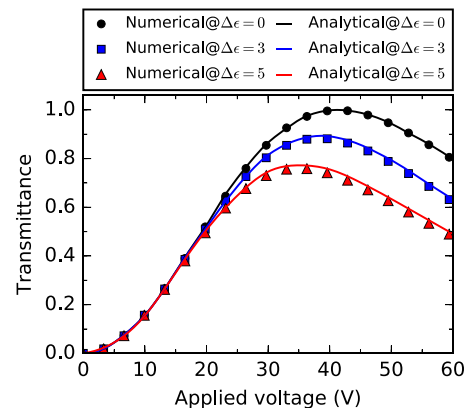


FIG. 6. Simulated VT curves from numerical macroscopic model and analytical equation (10). The material parameters are listed in Table I.

Normally, we focus on the peak transmittance and the corresponding voltage. But one needs to notice that the applied voltage also depends on the cell gap. To exclude other influences from the LC material itself, we use on-state rotation angle to represent the applied voltage. The corresponding on-state voltage can be easily obtained from rotation angle by Eq. (2). The simulated maximum transmittances and on-state rotation angles of all these different materials are then plotted in Figs. 7(a) and 7(b). Each point in Fig. 7 represents a LC material.

The simulated maximum transmittance of these different LC materials perfectly lie on a smooth curve in Fig. 7(a), and so do on-state rotation angle. That means our definition of *FOM* in Eq. (11) is reasonable. When there is no dielectric coupling, the maximum transmittance can achieve $\sim 100\%$ at 45° rotation angle, because the ULH cell works as a half-wave plate in this case. As dielectric coupling gets stronger, the peak transmittance occurs at a lower voltage and the maximum transmittance decreases, as shown in Fig. 4. The transmittance reaches maximum before the rotation angle gets to 45° . Therefore, in Fig. 7, as the *FOM* increases with stronger flexoelectric effect and weaker dielectric coupling, both maximum transmittance and on-state rotation angle increase and then gradually saturate. The relationship between VT behavior and *FOM*, presented in Fig. 7, is useful for optimizing LC materials. Some special points are annotated in Fig. 7. For instance, to keep maximum transmittance over 95%, the LC material should have a *FOM* larger than 3.1. Although dielectric coupling lowers the peak transmittance, it helps reduce the on-state voltage as Fig. 7(b) depicts. For instances, if $FOM = 2.6$, the on-state rotation angle is 42.0° , whose on-state voltage is 90% compared to the ULH with purely flexoelectric effect, but the peak transmittance drops to 92%. Similarly, if $FOM = 1.3$, then the on-state voltage is reduced by $\sim 20\%$, but the peak transmittance is also decreased by $\sim 20\%$.

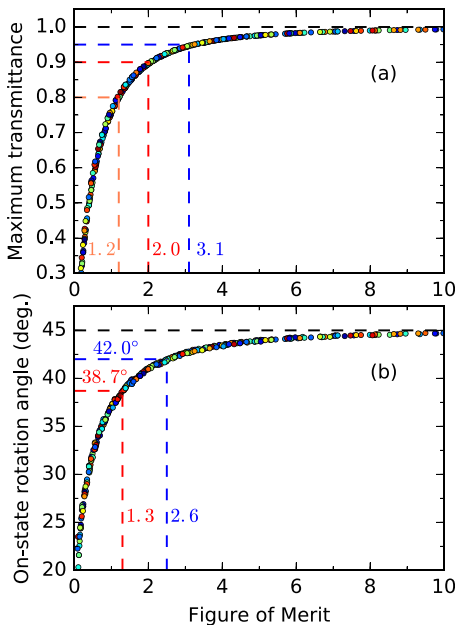


FIG. 7. Relationship between VT behavior and *FOM* of different LC materials: (a) maximum transmittance and (b) on-state rotation angle.

TABLE II. The LC material recipes of three ULH samples.

	Samples		
	S1 (%)	S2 (%)	S3 (%)
TL213	37.0	46.4	23.3
UCF-N1	9.2	0	0
E48	0	0	22.1
FFE7EFF	46.3	46.4	47.1
R5011	4.0	4.0	4.1
RM257	2.9	2.9	3.1
Ir651	0.6	0.3	0.3

III. EXPERIMENT

A. Sample preparation

To verify the theoretical prediction from our macroscopic model, we formulated three ULH LC mixtures to experimentally investigate the dielectric coupling effect. The compositions of the LC mixtures are listed in Table II. The first three mixtures were used as nematic hosts. The dielectric anisotropy of TL213 (Merck), UCF-N1, and E48 (Merck) are 5.7, -4.0 , and 15.4, respectively. To verify the dielectric coupling effect, we changed the weight ratios of these three LC hosts in order to get different $\Delta\epsilon$ values. The bimesogenic material FFE7EFF was used to offer large flexoelectric effect. The ester-linked symmetric bimesogen FFE*n*EFF homologues [α -(2', 4-difluorobiphenyl-4'-ester)- ω -(4-difluorobiphenyl-4'-ester) alkanes] were demonstrated to have relatively large flexoelectric coefficient (~ 1.7 C/N/m).¹⁷ During experiment, we tried to keep the FFE7EFF concentration unchanged in order to maintain the flexoelectric effect of these three samples at the same level. We added ~ 4 wt. % chiral dopant R5011 (HCC) to get the CLC pitch length $p \approx 200$ nm. Mesogenic monomer RM257 (Merck) and photoinitiator Ir651 were doped into the mixtures in order to stabilize the ULH alignment by polymer network.

These three LC mixtures were expected to have similar flexoelectric effect and pitch length due to the same FFE7EFF and R5011 concentrations. Thus, their electrooptic behaviors should only be different in dielectric effect. The measured dielectric anisotropy and pitch length are listed in Table III. In our experiments, we used conventional homogeneous (HG) LC cells with planar top and bottom ITO electrodes. The cell gaps are also included in Table III.

TABLE III. Measured dielectric anisotropy, pitch length, cell gap, and contrast ratio of our 3 ULH samples.

	Samples		
	S1	S2	S3
Dielectric anisotropy ^a	~ 0	1.14	5.09
Pitch length	198 nm	189 nm	194 nm
Cell gap	3.28 μm	3.25 μm	3.41 μm
Contrast ratio	240:1	180:1	145:1

^aMeasured dielectric anisotropy of the host mixtures and bimesogenic materials.

Before we characterize the electro-optic properties of these cells, we need to obtain good uniform lying helix. Many alignment methods have been proposed to generate ULH pattern, for instance, cooling CLC with applied voltage,^{10,24,31,32} mechanical shearing,^{12,33} and tri-electrode method.³⁴ In our experiment, we used the blue phase to ULH transition method to obtain ULH pattern. After cooling the samples from isotropic phase to blue phase, by applying a 500 Hz AC electric field, a preliminary ULH alignment was generated. Afterwards, we switched the frequency to ~ 20 kHz and then further increased voltage to obtain a much better ULH alignment. The images of ULH texture under polarizing optical microscope (POM) are shown in Fig. 8. It is critical not to apply a too high voltage, otherwise the ULH pattern could turn into homeotropic alignment, and we have to heat up the sample to an isotropic phase and repeat the process. After uniform alignment has been obtained, we need to stabilize the ULH pattern using polymer network.

In our experiments, the polymer network was formed and localized near the surface of substrates. Compared with bulk polymer network, the surface polymer network can help reduce the residual birefringence and polymer bulk defects.^{23,35} The polymerization was performed with voltage applied, by exposing the cell with ultraviolet light intensity 30 mW/cm^2 for 5 min. With this method, we were able to align ULH samples with a reasonably high contrast ratio (CR) [Table III].

The surface alignment achieved by the surface localized polymer network helps maintain the ULH pattern after removing the alignment electric field. With the help of polymer network, the ULH cells can be operated in a relative wide temperature range, at least $20\text{--}60^\circ\text{C}$. All our cells were measured at room temperature ($\sim 20^\circ\text{C}$). Also, our cells showed good long-term stability of the ULH pattern with the surface localized polymer network, and kept a relatively high contrast ratio within the working temperature range. The surface alignment is necessary for maintaining the well-aligned ULH pattern, but it also creates some issues: (1) It would increase the operation voltage, and (2) the adoption of surface alignment would reduce the effective thickness of ULH cell because of the inactive surface layer. The periodic surface localized polymer fibers have diameter of about $50\text{--}100 \text{ nm}$ at the substrate surfaces.²³

B. Results and discussion

To confirm the flexoelectric modulation in our samples, we first measured the in-plane rotation of the CLC helix. The

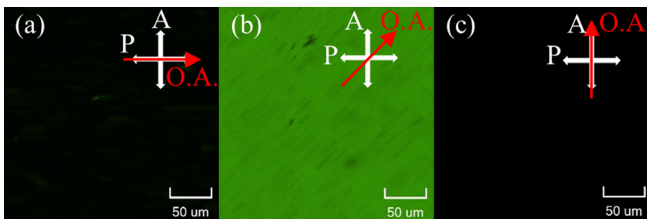


FIG. 8. Images of ULH texture under polarizing optical microscope (POM): (a) ULH optical axis (O.A.) at 0° with respect to the polarizer; (b) at 45° and (c) at 90° .

samples were driven by a 60 Hz square-waveform AC electric field, and placed between two crossed polarizers. The initial orientation of optic axis of the sample was set to be parallel to the polarizer, as shown in Fig. 8(a). With the voltage applied, the induced rotation can be measured by rotating sample to the extinction position.²⁴ The measured rotation angles of these three samples are plotted in Fig. 9, where the approximate linear relationships are clearly illustrated in Figs. 9(a) and 9(b). While in Fig. 9(c), the rotation angle shows a slight decrease at the high voltage region, which is induced by dielectric coupling as clearly shown in Fig. 3. In the small angle limit, Eq. (2) can be approximated as

$$\tan \Psi \approx \frac{p}{2\pi} \frac{e_s - e_b}{K_{11} + K_{33}} E. \quad (12)$$

This equation was then used to fit the linear region of the measured rotation angle versus applied voltage, as shown in Fig. 9. Note that the effective thickness of ULH is slightly smaller than the cell gap, because of the existence of the inactive surface LC layer. In our fitting, considering the cell gap ($\sim 3.3 \mu\text{m}$) is much thicker than the inactive layer, we can ignore the inactive layer thickness for simplification. The extracted effective flexoelectric coefficients are listed in the figure caption. Three samples have similar rotation responses and flexoelectric coefficients, which means they should have same strength of the flexoelectric effect. These results are basically consistent with our LC material recipes.

Next, we measured the VT curves of the ULH cells sandwiched between two crossed polarizers. The results are plotted in Fig. 10. The measured maximum transmittance

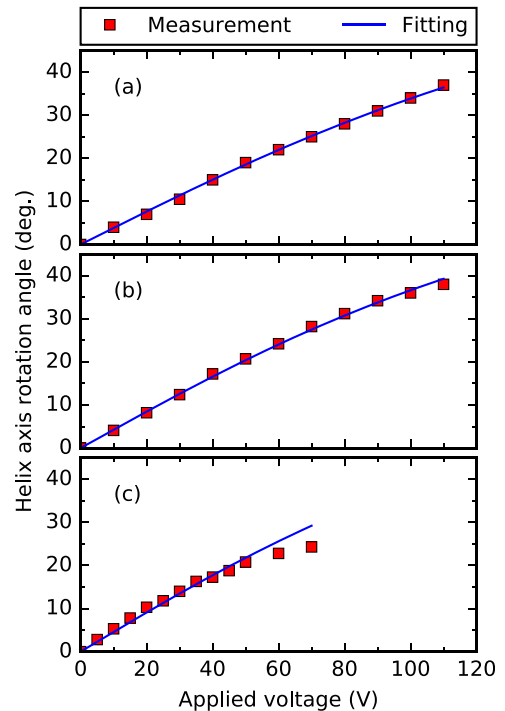


FIG. 9. Measured rotation angle of the CLC helix axis of three samples and respective fitting results. (a) Sample 1 with $(e_s - e_b)/(K_{11} - K_{22}) = 0.70 \text{ C/N/m}$, (b) sample 2 with $(e_s - e_b)/(K_{11} - K_{22}) = 0.80 \text{ C/N/m}$, and (c) sample 3 with $(e_s - e_b)/(K_{11} - K_{22}) = 0.88 \text{ C/N/m}$.

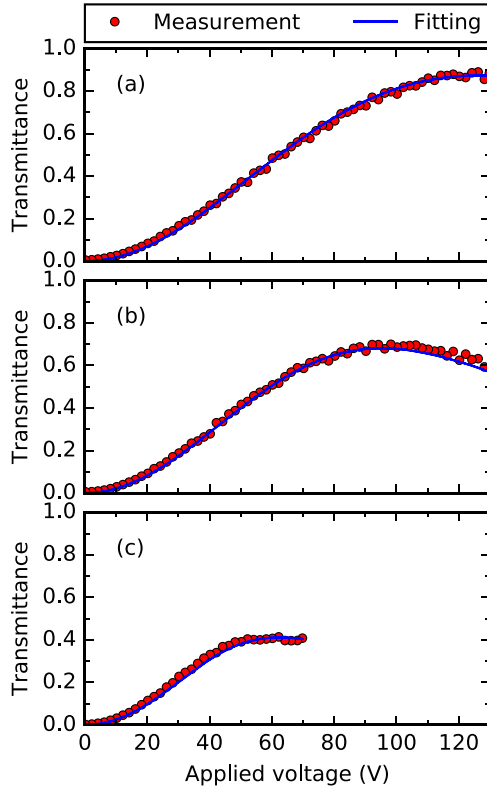


FIG. 10. Measured VT curves of three samples and the theoretical fitting results. (a) Sample 1 with fitting parameter $\Delta\epsilon/(K_{11} + 2K_{22} + K_{33}) = 0.028 \text{ C/N/m}$; (b) sample 2 with $\Delta\epsilon/(K_{11} + 2K_{22} + K_{33}) = 0.083 \text{ C/N/m}$; (c) sample 3 with $\Delta\epsilon/(K_{11} + 2K_{22} + K_{33}) = 0.410 \text{ C/N/m}$.

and on-state rotation angle are listed in Table IV. A clear trend is presented from the figures. As the dielectric coupling increases, namely, from sample 1 to sample 3, both maximum transmittance and on-state voltage decrease accordingly. This trend is consistent with our theoretical prediction. Moreover, we used Eq. (10) to fit the experimental VT curves and obtained excellent agreement, as shown in Fig. 10. Through fittings, we extracted the dielectric effect parameter $\Delta\epsilon/(K_{11} + 2K_{22} + K_{33})$, as indicated in the figures. With the fitted flexoelastic coefficients and dielectric parameters, the *FOMs* of three samples are calculated and results are listed in Table IV.

To further verify our theoretical predictions, we plot the maximum transmittance and on-state voltage of three samples in the *FOM* figure shown in Figs. 11(a) and 11(b), respectively. Again, the agreement is excellent. Thus, our proposed macroscopic model is validated experimentally.

In addition to transmittance and operation voltage, response time is another important parameter. In the experiment, we

TABLE IV. Measured maximum transmittance and rotation angle of our three ULH samples.

	Samples		
	S1	S2	S3
Figure of merit	2.01	0.88	0.21
Maximum transmittance (%)	90.36	70.39	42.10
On-state rotation angle (°)	40.4	35.8	22.8

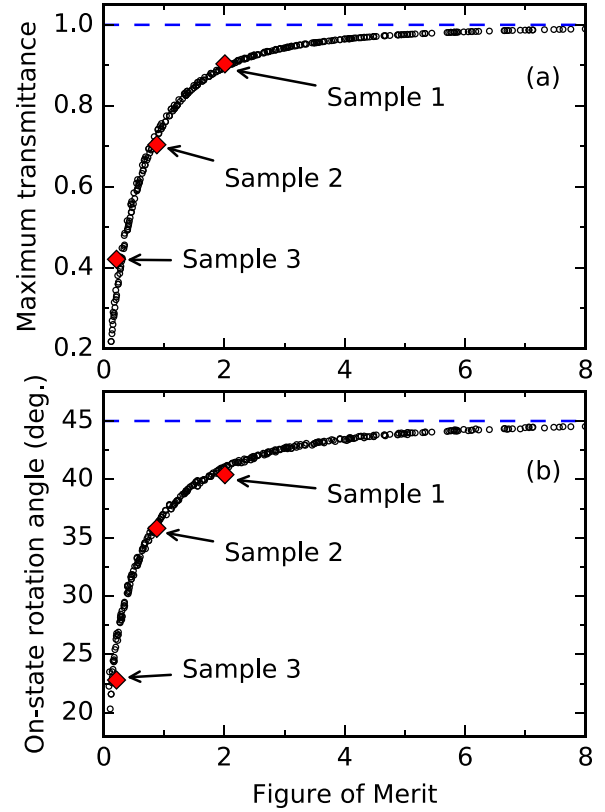


FIG. 11. Theoretical predictions and experimental results of (a) maximum transmittance and (b) on-state rotation angle for the 3 samples studied.

measured the response time of sample 1. Results are: rise time $262 \mu\text{s}$ (black-to-white) and decay time and $208 \mu\text{s}$ (white-to-black) at room temperature (22°C). We also measured the gray-to-gray (GTG) response time. To do so, we divided the VT curve into eight gray levels equally and measured the rise time and decay time between different gray levels. The GTG response time for all gray levels is below 1 ms. The measured average GTG rise time is $493 \mu\text{s}$ and decay time is $527 \mu\text{s}$.

For practical applications, the temperature effect on the device performance is an important issue. For the flexoelectric effect studied here, the effective flexoelectric coefficient and elastic constant of the LC materials have similar dependence on the temperature. As a result, according to Eq. (12), the in-plane rotation angle induced by the flexoelectric effect shows negligible sensitivity to the temperature variation.²³ Actually, the temperature-insensitive flexoelectric E-O switching in ULH cell has been experimentally demonstrated.^{12,23,24,33} As to the response time, the temperature dependence is similar to that of conventional nematic LCs. According to Eq. (3), γ/K decreases as the temperature increases, which in turn leads to faster response time. This phenomenon has already been observed in some previous experimental works.^{12,33}

As discussed above, the measured on-state voltage ($>100 \text{ V}$ for sample 1) is still too high for display applications. Such a high operation voltage originates from the LC material we employed. The extracted effective flexoelastic coefficient is only about 0.8 C/N/m . According to Eq. (12), to lower the operation voltage to below 20 V , the required flexoelastic coefficient should be $5\text{--}6\times$ higher than that of our samples. Recently, Merck reported two promising ULH

mixtures with operation voltages as low as 15.6 V and 19.2 V.³⁶ However, the response time (rise + decay) for the former is 5.9 ms, which is too slow for field sequential color display applications. The Merck results indicate that the ULH materials with a large flexoelectric coefficient (for low voltage) possess a relatively high viscosity (slow response time). Further material optimization is desperately needed.

Besides operation voltage, three other critical issues have to be overcome before widespread applications of ULH LCD can be realized: contrast ratio (CR), image flickering, and threshold voltage. The alignment uniformity of the ULH pattern has always been a big challenge, which in turn causes the light leakage in the dark state. At the present stage, the highest CR of the ULH mode reported is about <500:1. In comparison with conventional vertical alignment (VA) mode (CR ~ 5000:1) and fringe-field switching (FFS) mode (CR ~ 2000:1), ULH still has a long way to go. The second important issue is the image flickering in the ULH mode. For ULH cells driven by AC voltage, image flickering occurs when the polarity of the electric field is reversed, because the flexoelectric switching is dependent on the electric field polarity. Next, we examine the threshold voltage issue. From our experimental data [Fig. 10] and simulated VT curves [Fig. 4], the ULH mode does not seem to exhibit a threshold voltage. This could be a potential problem if ULH is intended for TFT LCD applications. For a high resolution display device, say, 3840 × 2160, millions of TFTs are fabricated. Each TFT could have up to 0.8 V voltage fluctuation. If ULH does not have a threshold voltage, then the dark state light leakage could occur. In the low voltage region where V is small, from Eq. (6) the first term (blue dashed lines in Fig. 4) is basically a constant and the transmittance is mainly governed by the second term (red dashed lines in Fig. 4). Under such circumstances, the transmittance of ULH can be approximated as

$$T \approx \left(\frac{2V}{V_{on}} \right)^2, \quad (13)$$

where V_{on} is the voltage corresponding to the peak transmittance. From Eq. (13), there is no threshold voltage for the ULH mode. Thus, any voltage fluctuation from TFTs could cause light leakage in the dark state. This could be a serious issue of the ULH mode for display applications.

IV. VIEWING ANGLE

The ULH CLC offers high transmittance and sub-millisecond response time, but its viewing angle needs to be analyzed as well. In the present work, we simulate the ULH viewing angle by two numerical methods: (1) through LC director distributions and (2) utilizing our macroscopic model. The macroscopic approximation is found to be an efficient and fast method for viewing angle simulation.

We first solve the Euler-Lagrange equations as described in Sec. II to obtain the LC director distribution in one pitch. In order to construct the LC directors in the whole cell, we need to extend the CLC pitches and uniformly align the helix axes. Next, we simulate the optical performance

using 2×2 extended Jones matrix method.³⁷ The LC director distribution in one pitch is shown in Fig. 1. Because of the short pitch length, the calculation mesh size must be fine enough to get good accuracy. Therefore, the computing time increases dramatically. This is one of the major difficulties to calculate the ULH viewing angle using conventional method. Figure 12(a) shows the simulated isocontrast

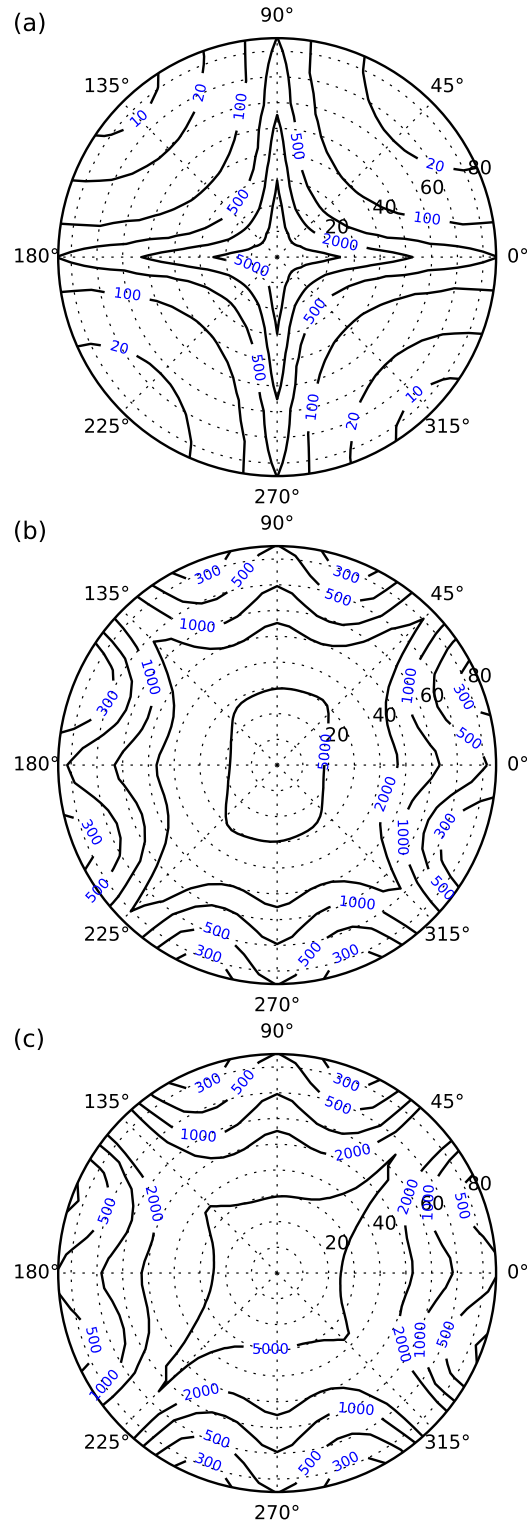


FIG. 12. Simulated ULH isocontrast contours using conventional method: (a) uncompensated; (b) with one +A and one +C compensation films; and (c) with a biaxial compensation film.

contour of a ULH cell sandwiched between two crossed polarizers. To be consistent, the parameters used in the simulation are also from Table I. Without losing generality, we chose the wavelength at 550nm. The simulated isocontrast contour is quite similar to that of conventional in-plane switching (IPS) or fringe-field switching (FFS) cell.^{38,39} This is the first quantitative demonstration that ULH exhibits a similar viewing angle to IPS.

To further widen the viewing cone of ULH, we can adopt compensation films. Due to their structural similarities, the compensation films used in IPS should also work well for ULH. We first use two uniaxial films:⁴⁰ one +A plate ($n_e = 1.5110$, $n_o = 1.5095$, and thickness $92.59 \mu\text{m}$) and one +C plate ($n_e = 1.5110$, $n_o = 1.5095$, and thickness $60.09 \mu\text{m}$). For practical applications, to reduce the total panel thickness while keeping wide viewing angle, we prefer to use a half-wave biaxial film, whose parameters are $n_x = 1.521$, $n_y = 1.519$, $n_z = 1.520$, and thickness is $137.5 \mu\text{m}$.⁴¹

Figures 13(a) and 13(b) depict the device configurations using uniaxial films and biaxial film, respectively. The simulated iso-contrast contours are plotted in Figs. 12(b) and 12(c). After compensation, the viewing angle of ULH LC cell is relatively symmetric and the viewing cone with $\text{CR} > 300:1$ is over 85° . The compensated viewing angle of ULH is more symmetric than the compensated IPS or FFS. This difference is caused by the small pre-tilt angle in the IPS cell and different working mechanisms involved. The ULH cell implements uniform in-plane rotation, while IPS and FFS

mode would exhibit two twisted LC director distribution along the longitudinal direction.^{38,40}

Next, we simulated the viewing angle of ULH LCDs with or without compensation films using macroscopic model. The ULH LC layer can be simplified to a uniaxial layer or a biaxial layer with effective refractive indices and orientation obtained from above macroscopic model. In the

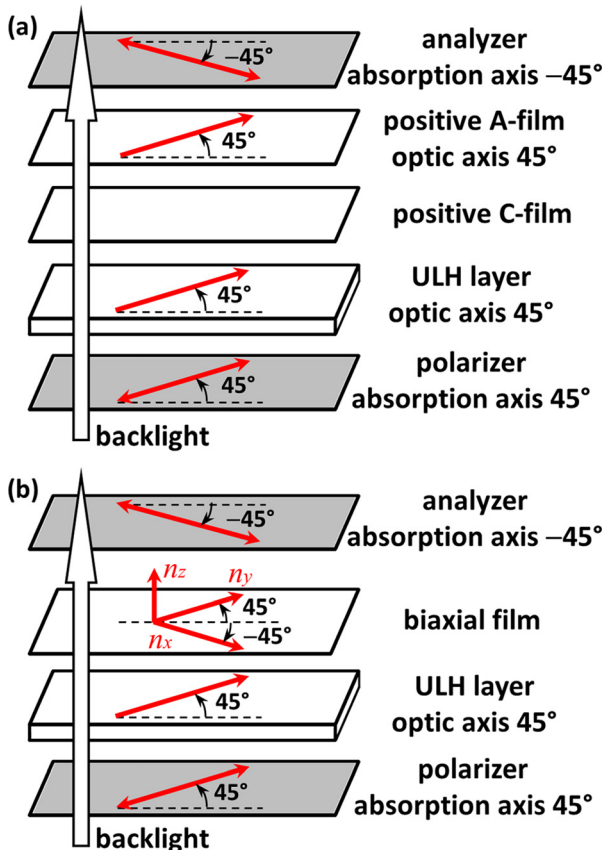


FIG. 13. Device configurations of ULH cell with compensation films: (a) one +A and one +C compensation film, and (b) one biaxial compensation film.

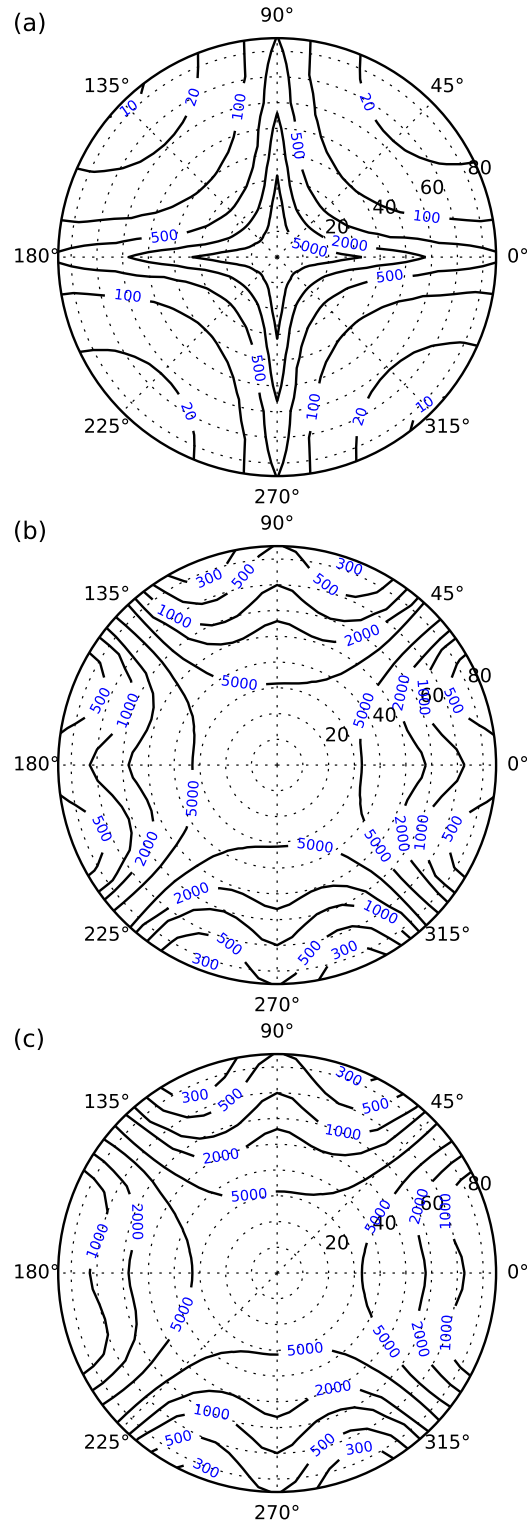


FIG. 14. Simulated ULH isocontrast contours using macroscopic model: (a) uncompensated; (b) with one +A and one +C compensation films; and (c) with a biaxial compensation film.

optical simulation of biaxial layer, we need to reconstruct the dielectric tensor, which is different from conventional uniaxial nematic LC simulation. The simulated results are shown in Fig. 14. In comparison with Fig. 12, we find that the macroscopic model gives quite similar results to that from conventional one, especially in the $CR < 2000:1$ region. Moreover in macroscopic model, ULH is simplified to one uniaxial or biaxial film, which helps to greatly reduce the computing time by more than 10 times in our simulations.

V. CONCLUSION

We have investigated the flexoelectric effect and dielectric effect in short-pitch ULH CLCs both theoretically and experimentally. Our proposed macroscopic optical model is proven to be a useful tool to understand the optical behaviors of the flexoelectric effect and dielectric effect, and to quantitatively analyze the interaction of these two E-O effects. From the basic LC physics, a figure of merit is derived to evaluate the relative strength of the flexoelectric effect and the dielectric effect. The theoretical prediction has been validated by both numerical simulation and experimental measurement. Finally, we simulated the viewing angle of a uniform lying helix CLC display and found that its viewing angle characteristics are similar to those of IPS LCDs.

ACKNOWLEDGMENTS

The authors are indebted to Haiwei Chen for useful discussion and a.u.Vista, Inc., for financial support.

¹M. Schadt, *Jpn. J. Appl. Phys.* **48**, 03B001 (2009).

²K. Bourzac, *Nature* **493**, 283 (2013).

³Z. Luo, Y. Chen, and S.-T. Wu, *Opt. Express* **21**, 26269 (2013).

⁴H. Chen, F. Peng, F. Gou, Y. H. Lee, M. Wand, and S.-T. Wu, *Optica* **3**, 1033 (2016).

⁵F. Peng, H. Chen, F. Gou, Y. H. Lee, M. Wand, M. C. Li, S. L. Lee, and S.-T. Wu, *J. Appl. Phys.* **121**, 023108 (2017).

⁶H. Kikuchi, M. Yokota, Y. Hisakado, H. Yang, and T. Kajiyama, *Nat. Mater.* **1**, 64 (2002).

⁷Z. Ge, S. Gauza, M. Jiao, H. Xianyu, and S.-T. Wu, *Appl. Phys. Lett.* **94**, 101104 (2009).

⁸Y. Haseba, H. Kikuchi, T. Nagamura, and T. Kajiyama, *Adv. Mater.* **17**, 2311 (2005).

⁹R. B. Meyer, *Phys. Rev. Lett.* **22**, 918 (1969).

¹⁰J. S. Patel and R. B. Meyer, *Phys. Rev. Lett.* **58**, 1538 (1987).

¹¹F. Castles, S. M. Morris, and H. J. Coles, *Phys. Rev. E* **80**, 031709 (2009).

¹²P. Rudquist, M. Buivydas, L. Komitov, and S. T. Lagerwall, *J. Appl. Phys.* **76**, 7778 (1994).

¹³S. D. Lee, J. S. Patel, and R. B. Meyer, *J. Appl. Phys.* **67**, 1293 (1990).

¹⁴P. Rudquist, L. Komitov, and S. T. Lagerwall, *Phys. Rev. E* **50**, 4735 (1994).

¹⁵S. J. Elston, *Phys. Rev. E* **78**, 011701 (2008).

¹⁶J. S. Patel and S.-D. Lee, *J. Appl. Phys.* **66**, 1879 (1989).

¹⁷S. M. Morris, M. J. Clarke, A. E. Blatch, and H. J. Coles, *Phys. Rev. E* **75**, 041701 (2007).

¹⁸C. H. Chen, F. C. Lin, Y. T. Hsu, Y. P. Huang, and H. P. D. Shieh, *J. Disp. Technol.* **5**, 34 (2009).

¹⁹Y. Huang, H. Chen, G. Tan, H. Tobata, S.-I. Yamamoto, E. Okabe, Y. F. Lan, C. Y. Tsai, and S. T. Wu, *Opt. Mater. Express* **7**, 641 (2017).

²⁰A. Buka and N. Eber, *Flexoelectricity in Liquid Crystals: Theory, Experiments and Applications* (World Scientific, 2012), pp. 211–248.

²¹B. Musgrave, P. Lehmann, and H. J. Coles, *Liq. Cryst.* **26**, 1235 (1999).

²²H. J. Coles, M. J. Clarke, S. M. Morris, B. J. Broughton, and A. E. Blatch, *J. Appl. Phys.* **99**, 034104 (2006).

²³A. Varanytsia and L. C. Chien, *J. Appl. Phys.* **119**, 014502 (2016).

²⁴R. Balachandran, V. P. Panov, J. K. Vij, A. Lehmann, and C. Tschierske, *Phys. Rev. E* **88**, 032503 (2013).

²⁵D. R. Corbett and S. J. Elston, *Phys. Rev. E* **84**, 041706 (2011).

²⁶C. Oldano and M. Rajteri, *Phys. Rev. B* **54**, 10273 (1996).

²⁷P. Hubert, P. Jagemalm, C. Oldano, and M. Rajteri, *Phys. Rev. E* **58**, 3264 (1998).

²⁸J. Yan, H.-C. Cheng, S. Gauza, Y. Li, M. Jiao, L. Rao, and S.-T. Wu, *Appl. Phys. Lett.* **96**, 071105 (2010).

²⁹P. R. Gerber, *Mol. Cryst. Liq. Cryst.* **116**, 197 (1985).

³⁰B. I. Outram and S. J. Elston, *Liq. Cryst.* **40**, 1529 (2013).

³¹B. I. Outram and S. J. Elston, *Appl. Phys. Lett.* **103**, 141111 (2013).

³²C. Wang, W. Wang, and T. Lin, *Appl. Phys. Lett.* **99**, 041108 (2011).

³³P. Rudquist, L. Komitov, and S. T. Lagerwall, *Liq. Cryst.* **24**, 329 (1998).

³⁴D. J. Gardiner, S. M. Morris, P. J. W. Hands, F. Castles, M. M. Qasim, W.-S. Kim, S. S. Choi, T. D. Wilkinson, and H. J. Coles, *Appl. Phys. Lett.* **100**, 063501 (2012).

³⁵S. H. Kim, L. C. Chien, and L. Komitov, *Appl. Phys. Lett.* **86**, 161118 (2005).

³⁶S. Siemianowski, M. Bremer, E. Plummer, B. Fiebranz, M. Klasen-Memmer, and J. Canisius, *Tech. Dig. - SID Symp. Pap.* **47**, 175 (2016).

³⁷A. Lien, *Appl. Phys. Lett.* **57**, 2767 (1990).

³⁸S. H. Lee, S. L. Lee, and H. Y. Kim, *Appl. Phys. Lett.* **73**, 2881 (1998).

³⁹Y. Saitoh, S. Kimura, K. Kusafuka, and H. Shimizu, *Jpn. J. Appl. Phys., Part 1* **37**, 4822 (1998).

⁴⁰X. Zhu, Z. Ge, and S. T. Wu, *J. Disp. Technol.* **2**, 2 (2006).

⁴¹Q. Hong, T. X. Wu, R. Lu, and S. T. Wu, *Opt. Express* **13**, 10777 (2005).